Journal of Adhesion Science and Technology

ISSN: 0169-4243 (Print) 1568-5616 (Online) Journal homepage: https://iom3.tandfonline.com/loi/tast20

Characterization of superficial modification of ferrous rusted substrates subjected to dechlorination-electrochemical process

R. Parra, A. Covelo, R. J. Ramírez, A. Tejeda, A. Ortega & M. Hernández

To cite this article: R. Parra, A. Covelo, R. J. Ramírez, A. Tejeda, A. Ortega & M. Hernández (2018) Characterization of superficial modification of ferrous rusted substrates subjected to dechlorination-electrochemical process, Journal of Adhesion Science and Technology, 32:12, 1341-1358, DOI: 10.1080/01694243.2017.1409854

To link to this article: https://doi.org/10.1080/01694243.2017.1409854

JOURNAL OF ADHESION SCIENCE AND TECHNOLOGY, 2018
VOL. 32, NO. 12, 1341–1358
https://doi.org/10.1080/01694243.2017.1409854

Taylor & Francis
Taylor & Francis Group

Characterization of superficial modification of ferrous rusted substrates subjected to dechlorination-electrochemical process

R. Parra[a], A. Covelo[a], R. J. Ramírez[a], A. Tejeda[b], A. Ortega[c] and M. Hernández[a]

[a]Facultad de Ingeniería, Depto. de Materiales y Manufactura. Centro de Ingeniería de Superficies y Acabados (CENISA), Universidad Nacional Autónoma de México (UNAM), 04510, México; [b]Instituto de Investigaciones en Materiales. Universidad Nacional Autónoma de México (UNAM), 04510, México; [c]Instituto de Ciencias Nucleares. Universidad Nacional Autónoma de México (UNAM), 04510, México

ABSTRACT

Preservation of archaeological artefacts after their removal from saline media is a difficult task due to the chloride content of the oxide layers which are unstable in atmospheric conditions, especially if the relative humidity exceeds 85%. For this reason, removal of chlorides from rust layers is one of the priorities of conservationists or restorers of historical artefacts. However, removal of chloride ions is not an easy procedure because of the many considerations involved in the process. In this research, artificially pre-rusted iron samples and an actual historical cannonball were subject to a dechlorination process in a potassium hydroxide solution to measure constant chloride release in a bulk solution. After the chloride removal process, a commercial protective layer was applied to the rust for stabilization purposes. It was calculated that the kinetics of the dechlorination process is driven by diffusion behaviour following Fick's second law. When this diffusion process prevails, the dechlorination extraction affects the integrity of rust layers as is demonstrated with scanning electron microscopy and X-ray diffraction analyses. It was proven that the chloride removal procedure causes the studied iron layers to stiffen, provoking superficial modification and, in some cases, fractures of the rust. By means of electrochemical impedance spectroscopy it was calculated that the magnitude of the positive effect of the dechlorinated samples depends on the protective features of the rust. Therefore, this research reveals that an efficient chloride removal procedure depends on the electrochemical properties of the dechlorination process and the initial morphology of the iron rust.

ARTICLE HISTORY
Received 14 July 2017
Revised 15 October 2017
Accepted 22 November 2017

KEYWORDS
Carbon steel; SEM; X-ray diffraction; rust; dechlorination

Introduction

Archaeological rusted ferrous materials found in marine conditions have been subject to aggressive media for many decades resulting in the formation of chloride corrosion products covering the ferrous substrate entirely. Chloride from the marine environment is held in

CONTACT M. Hernández mahdz2010@comunidad.unam.mx

artefacts as counter-ions [1] and a range of chloride-bearing corrosion products are formed [2] over the years. In post-excavation the hydrolysis and oxidation of ferrous ions in artefacts produces voluminous corrosion products which damage the corrosion product layers that contain evidence of the object's shape [1] given that the atmospheric air interacts with the artefacts generating fractures or swelling. In addition, the chloride content within the corrosion layers keeps degrading the metallic substrate, regardless of the nature or composition of the oxides. For this reason, several research projects have focused their attention on desalination through the dechlorination process as an effective alternative to stabilize the rust of corroded artefacts [3–8]. However, besides the chloride content, studies have also reported that ferrous ions also react in the presence of air, resulting in further corrosion activity. Depending on the nature of the artefacts, the iron rust could be in the form of either a hydroxide-like compound or, as already indicated, an iron phase [8,9]. For this reason, the removal and quantification of the ferrous ion should also be carefully considered [10,11], as well as the chloride anion profile within rusted artefacts [12]. It is reported in the literature that chloride-containing artefacts should reach an optimal extraction of 95% of chloride ions in order to stabilize the artefact [9] regardless of the combination of variables such as treatment times, temperature and the initial concentration of chloride ion [13–15]. However, such conditions are difficult to achieve since other parameters affect the extraction procedure, such as different chloride concentrations within the artefact, porosity and the physical condition of the corrosion products. These conditions result in a non-uniform extraction procedure; thus, it is suggested that the dechlorination process ceases when the chloride ion concentration in the bulk solution is lower than 50 ppm. In order to increase the chloride diffusion, past treatments involving alkaline washings [4] and reduction of corrosion layers have led [16–19] to higher extraction efficiency.

Nevertheless, this study focuses on electrolysis to remove soluble chloride and, for this reason, solutions used during the chloride extraction should be taken into account. Solutions such as sodium hydroxide, alkaline sulfite, sodium sesquicarbonate as well as alcoholic hydroxides are the most common electrolytes used for this purpose [20–22]. Changing the oxide density affects not only morphological features but also results in chemical interactions such as adhesion forces between the oxide layer and the metal substrate [22]. In spite of an adequate solution selection, the success of the dechlorination process relies on determining the final solution chloride concentration as well as measuring the chloride extraction during treatment [23]. However, the dechlorination process via electrochemical reaction does not guarantee that all chlorides are removed from the corrosion layers and thus other attempts have been developed to increase the chloride extraction efficiency; these methods involve sub-critical conditions of pressure and temperature [24–26]. Such studies seem to be promising although parameters such a pH solution, temperature control, eluent flow, processing time and the types of corrosion layers need to be further investigated [25].

In order to provide further tools to understand the dechlorination phenomenon, this paper estimates the diffusion behaviour of chloride anions during the dechlorination process and its effects on the microstructural features of ferrous rusted substrate, with the objective of proving the morphology modification of artefacts that have been artificially rusted and those that have naturally rusted (historical artefacts) under seawater conditions.

Experimental

Materials

Commercial low carbon steel samples of 7.5 cm × 5 cm × 1 mm were cut, ground with silicon carbide paper using grit-220 followed by a wash with distilled water, degreased with acetone and dried under an air flow. These samples were subject to constant spray humidification using synthetic ocean water with a salt spray fog chamber with specifications according to ASTM D1141 [27] over a period of 10 to 15 weeks in order to generate thick corrosion products. This procedure led to the build-up of artificial marine rust with different thicknesses that were measured with an Extech Instruments CG204 Ultrasonic Thickness Gauge. After the rusting procedure, the samples were cut into smaller coupons leaving an exposed area of 2 cm^2 for the dechlorination process. In addition, an authentic historical cannonball from the San Juan de Ulúa Fort (Veracruz, Mexico) was also used for the chloride extraction procedure using the same area of 2 cm^2.

The elemental composition of rusted samples was determined by using an XRF analyzer Bruker S1-Titan.

Characterization techniques

Chloride extraction procedure

The polarization potential (constant reduction) for the chloride extraction process was established at –1.2 V/SCE in a potassium hydroxide solution (1 M) in accordance with previous polarization results (Figure A1 in Appendix 1). The current density of the test was ≈ 5 mA/cm^2. This potentiometry was conducted using a stable power supply. A solid copper wire attached to the samples (cathodes) was connected to the negative polarity of the power supply while a platinum mesh (anode) surrounding the samples was connected to the positive plug. A saturated calomel electrode (SCE), coupled with the cathode, monitored the polarized potential. Since the artificially rusted substrates (ARS) and the historical cannonball (HCB) had different chloride concentrations within the corrosion layers, a standard criterion of chloride removal was prepared for both cases. This consisted of measuring a constant chloride concentration (mg) in a bulk solution which varied depending on the duration of the dechlorination process in each case. For the HCB, the constant average amount of chloride removal was approximately 0.75 g/l, while for the ARS it was approximately 5 g/l. These values were obtained by testing and measuring five samples in each case; therefore, these results offer statistical reproducibility. The chloride concentration was measured by using a chloride selective electrode with a ECM71 Hach device at room temperature. The procedure was as follows: in a 100 ml container of potassium hydroxide solution, with the electrochemical set-up as already described, the rusted samples were polarized for 24 h. Afterwards, the experiment was interrupted, the electrolysis solution was removed and by using the Hach device, the Cl^- concentration was measured a minimum of five times. Later, a new KOH solution was placed with the rusted samples and the dechlorination process continued for another 24 h. This cycle was repeated for 7 days. The Cl^- content in each aliquot was measured and, by adding the previous result to the new result, the total amount of chloride extracted from the rusted samples was calculated.

Electrochemical impedance

Electrochemical impedance spectroscopy (EIS) was used to verify the magnitude of the corrosion resistance of the rusted samples before and after the chloride removal. The electrochemical set-up consisted of rusted samples as working electrodes, a reference saturated calomel electrode (SCE) and a graphite rod as a counter-electrode. The sweeping frequency was from 10 kHz to 100 mHz with constant amplitude of 10 mV at open circuit potential (OCP). The EIS measurements were applied for 168 h. The electrolyte used in EIS testing was sodium chloride 0.1 M. Again, five samples in both cases were measured for reproducibility criterion.

Morphological and crystalline measurements

Scanning electron microscopy (SEM) and energy-dispersive X-ray (EDX) analyses were performed on the rusted samples in order to corroborate the effect of the dechlorination process before and after treatment. For this purpose an Electroscan JSM-54 model JEOL 5410 equipped with a Link ISIS 300 energy-dispersive X-ray detector was used. The surface roughness was measured by using a Mitutuyo SJ-310 (Kawasaki, Japan) mechanical profilometry device. At the same time, a Siemens D5000 X-ray diffraction (XRD) device equipped with copper radiation ($\lambda\alpha$ = 1.540 Å) from 2q = 5° to 2q = 85° was used on the crystalline features of the rusted layers. Finally, nanohardness measurements were carried out in order to corroborate the superficial modification of the samples after the dechlorination process. For this purpose, a Hysitron TI-750 UBi L Nano-Tester model along with a Berkovich indenter device was used. The load function took 25 s to load and 25 s to unload. At least three measures in several areas were performed for reproducibility criteria.

Protective/conservation product

In order to stabilize the dechlorinated surfaces, a commercial wax (Renaissance Wax) was applied to the iron layers. This solid micro-crystalline wax was heated until melted and applied with a soft brush onto the surface of the rusted layers. This product does not have an application data sheet for the amount or weight deposited on the surface. It contains isoparaffinic hydrocarbons and naphthenic hydrocarbons (with a high molecular weight) and also saturated aliphatic hydrocarbons.

Results and discussion

Table 1 shows the chemical composition (wt.%) obtained with SEM/EDX of the two materials (bare substrates) used in this investigation, the low carbon steel (ARS) and the historical cannonball (HCB). As expected, these two materials are completely different in their composition since the HCB corresponds to a grey cast iron category (%C:4.3) while the other is a very low carbon steel (SAE 1005). The physicochemical and metallographic characterization of the HCB is reported elsewhere [1]. Before the dechlorination process, these two objects were analyzed by means of fluorescence X-ray which gave the oxide compositions reported in Table 2. As can be seen, the oxides did not show a very different composition, most notably in their Fe, Si, P and Mn content, which means that from the metallurgical point of view both oxides are similar in their compositional profile.

Table 1. Chemical composition of the bare substrates (wt. %).

Composition of grey cast iron	C: 4.3; Si: 0.31, Mn: 0.145: S: 0.032, P:1.4, Ti: 0.023
Low carbon steel	C: 0.025; Si: 0.0016, Mn: 0.1935, S: 0.0127, P: 0.0162; Ti: 0.0026

Table 2. Fluoresce X-ray results (wt. %) of iron oxides.

Historical cannon ball (HCB)	Fe: 93.94; Si: 3.89; S:0.94; P:0.15; Mn: 0.26; Ti: 0.53; Ni: 0.08, Cu: 0.18, Sn: 0.03 Oxide average thickness (μm) = 366 ± 44.5
Artificially rusted simple (ARS)	Fe: 94.04; Si: 4.94; S:0.48; P:0.18; Mn: 0.15; Ti: 0.14; Ni: 0.04, Cu: 0.02, Al: 0.01 Oxide average thickness (μm) = 394 ± 12.5

Table 2 also shows the thickness of the ARS samples after 15 weeks of exposure to synthetic seawater, as well as the thickness of the HCB. All samples had similar values regarding the thickness of the corrosion products (oxide layers). It is clear that the initial morphology of the ARS is different (porous, non-compact) from the HCB rust layer, however, this difference is necessary in order to verify the influence of the chloride extraction on the structure. To corroborate that the ARS can simulate similar electrochemical behaviour to the HCB, a polarization curve was carried out in both cases with the bare substrate of the ARS. These results are illustrated in Figure A1 in (Appendix 1). A number of characteristics can be highlighted. The corrosion potential developed in both cases was between –0.75 and –0.9 V (SCE). For all systems, the cathodic region was governed by an activation zone followed by an incipient, limited current density at potentials of approximately –1.3 V. Therefore, at –1.2 V both cases are within the cathodic activation region. Nevertheless, above the corrosion potential (anodic direction) both cases showed a broad passive zone (–0.5 V to +1.5 V) constituted by different transition behaviours of passivation and repassivation. At potentials from +1.3 V to +1.5 V, both cases exhibited a pitting potential (Ep) above the oxygen evolution. Since this potential is approximately +0.458 V (SCE) at a pH of 13–14 (KOH 1 M), the Ep notably increased the current density. The bare metal substrate clearly showed the lowest current density as the potential became more positive, followed by the ARS and the HCB. These two cases had similar electrochemical behaviour along the entire polarization curve, i.e. the ARS reproduced the electrochemical features of the HCB. Therefore, taking into account the similarity between the average oxide thickness but, more importantly, the similarity in the oxide composition and the electrochemical properties, it is considered that comparing the corrosion products from the ARS and the HCB will allow for the study of the effects of the dechlorination process on the structural morphology in both cases.

After the dechlorination process, the amount of chlorides released for 144 h of testing in both cases (Figure 1) was calculated. From these results it can be observed that the chloride concentration displays a steep linear relationship with the square root of time (seconds$^{0.5}$). This behaviour indicates a process controlled by a diffusion law [28]. For the HCB this was true for up to 2 h of testing (509 s)$^{0.5}$ whereas, for the ARS, it was for up to 144 h (720 s)$^{0.5}$. Afterwards, the appearance of a constant plateau was measured, which meant there was no further removal of Cl^- from the rust layers, i.e. a stabilization process, where the concentration of chlorides released within the bulk solution is equal to the chloride concentration remaining on the iron rust layer of the metal; thus, in the absence of a driving force, the Cl^- extraction ceases [28]. From these results the *chloride extraction rate* was calculated (Figure 2) according to the following expression:

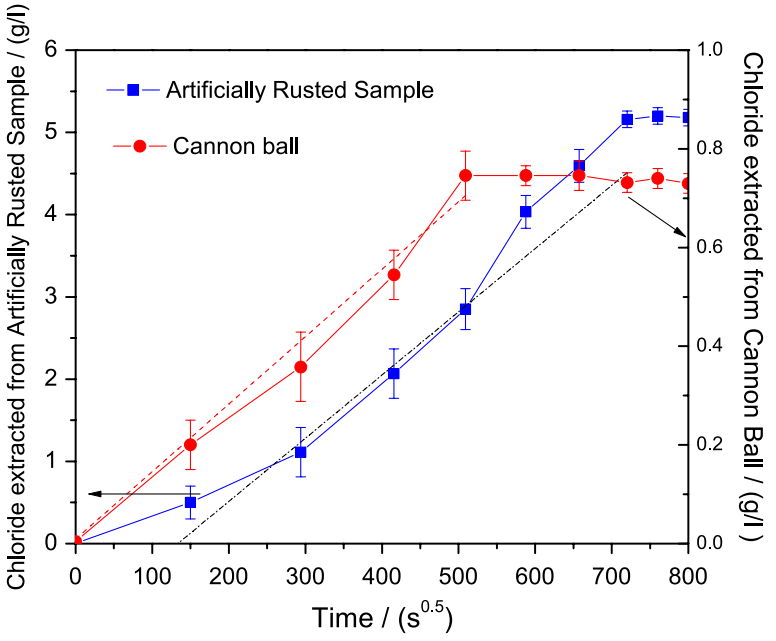

Figure 1. Amount of chloride extracted in NaOH solution as function of the square root of the time during the dechlorination process.

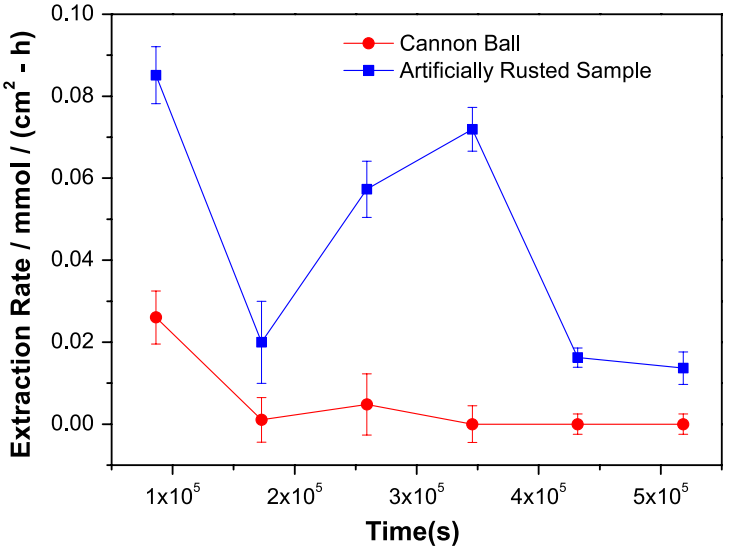

Figure 2. Extraction rates of chlorine anion during the dechlorination process.

$$r_{Cl} = \mathrm{d}Q_{Cl}/\mathrm{d}t \tag{1}$$

where $\mathrm{d}Q_{Cl}$ is the content of chloride anion extracted after a defined time and dt the extraction at a specific time [29] the extraction rate is expressed in mmol $(\mathrm{cm}^2\text{–h})^{-1}$

In general terms, the dechlorination rate decreased depending on the length of time given that the chloride anion concentration within the corrosion products diminished as the dechlorination process advanced. According to the literature, the extraction rate could also be enhanced by increasing the cathodic polarization potential of the dechlorination process [29]. Nevertheless, if this increase is obtained in the samples, it causes a higher hydrogen evolution due to the reduction in the reaction of water, which embrittles the iron rust. An increase in the chloride rate in both cases was observed. However, the ARS showed higher extraction rates compared with the HCB samples. The increase in the extraction rate after 2×10^5 s indicates superficial changes in the iron layer structure caused by dechlorination.

As described above, the kinetics of the dechlorination process (Figure 1) was controlled in a diffusion-like process via the oxide/metal interface for approximately 70 h of the process. The mobility of the ions in the presence of an electrical field gradient is described by the formal diffusion coefficient, D_{Cl}, of the system [30]. The D_{Cl} values were calculated according to Fick's second law, whose solution for an isotropic and semi-infinite diffusion system follows this expression:

$$C_x = C_o\left[1 - erf\left(\frac{x}{2\left(D_{Cl}t\right)^{1/2}}\right)\right] \tag{2}$$

where C_x is the remaining concentration of chloride anion within the corrosion products, C_o is the extracted chloride concentration in bulk solution, x is the rust average thickness, D is the formal diffusion coefficient and t is the time at specific extraction rate. Figure 3 depicts the evaluation of D_{Cl} according to expression 2. As can be seen, the extraction rates (Figure 2) and results from D_{Cl} (Figure 3) follow the same trend but, above all, the increase of the extraction rate is also reflected in the increase in the value of D_{Cl}. These results are consistent given that they indicate that the extraction rate depends not only on the amount

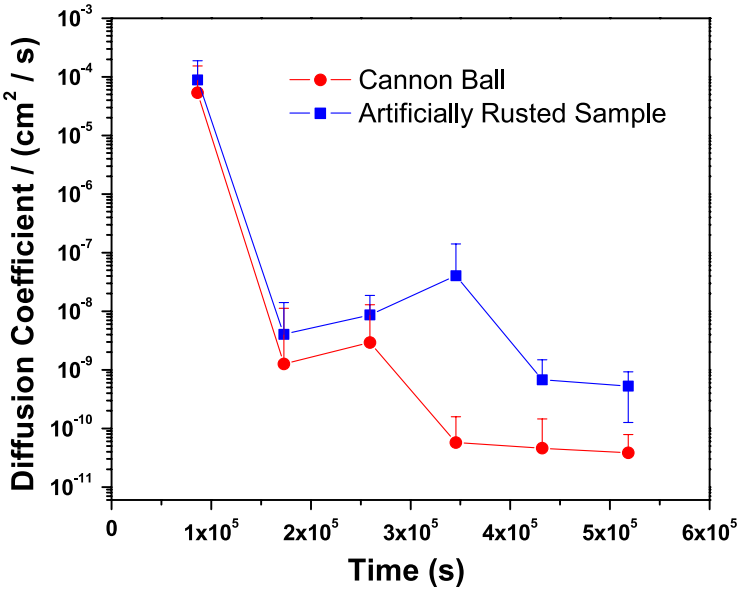

Figure 3. Calculation of D_{Cl}, formal diffusion coefficient, for both systems according to Fick's second law.

of chloride anions within the corrosion products but also depends on the Cl^- mobility expressed by the D_{Cl} in time. If D_{Cl} increases, then the chloride anion concentration gradient within the rust layers remains high. On the contrary, if D_{Cl} decreases, it is due mainly to a similar chloride anion concentration within the iron layer. Data from Figure 3 reveals a net decrease in the chloride anion diffusion coefficient from 8.89×10^{-5} to 5.26×10^{-10} $cm^2\ s^{-1}$ and from 5.34×10^{-5} to 3.82×10^{-11} $cm^2\ s^{-1}$ for the ARS and the HCB, respectively. If this experimental data of D_{Cl} at $t = 0$ is compared with the evaluation of D_{Cl} at infinite dilution (2.032×10^{-5} $cm^2\ s^{-1}$) [31] it can be observed that all values are similar, which indicates high Cl^- mobility within the iron rust at the beginning of the dechlorination process.

After the dechlorination process samples were covered with a commercial top-product (Renaissance Wax) to stabilize the oxide surface. This product is widely reported to work as an effective barrier layer on bronze and steel [32,33]. Its efficient anti-rust properties were studied and monitored using EIS [32] in long-term immersion testing. It was expected that the dechlorinated samples would have better corrosion performance in accordance with exhaustive literature results on the topic [4,5,8,26]. However, in order to measure the magnitude of the positive effect of the chloride extraction, EIS was conducted on both types of samples previously covered with the Renaissance Wax with and without a chloride content. Figure 4 depicts the Nyquist and the Bode impedance plots in the same graph after 168 h of testing. From the EIS spectra both cases indicate the presence of two time constants. In the Nyquist plots, at high frequencies, a capacitive-charge transfer behaviour associated with the response of the iron rust+wax of the samples is seen, whereas at low frequencies a larger semicircle caused by a corrosion process mechanism is shown.

The ARS showed higher resistance with and without chloride content, however, the impedance of the HCB was also sensitive after the dechlorination process. The iron rust+wax resistance ($R_{rust+wax}$ – Table 3) measured at high frequencies can be estimated from the electrical equivalent circuit used for modelling the EIS behaviour also illustrated in Figure 4, and consists of 2-RC time constants proposed by Murray et al. [34], where Rs refers to

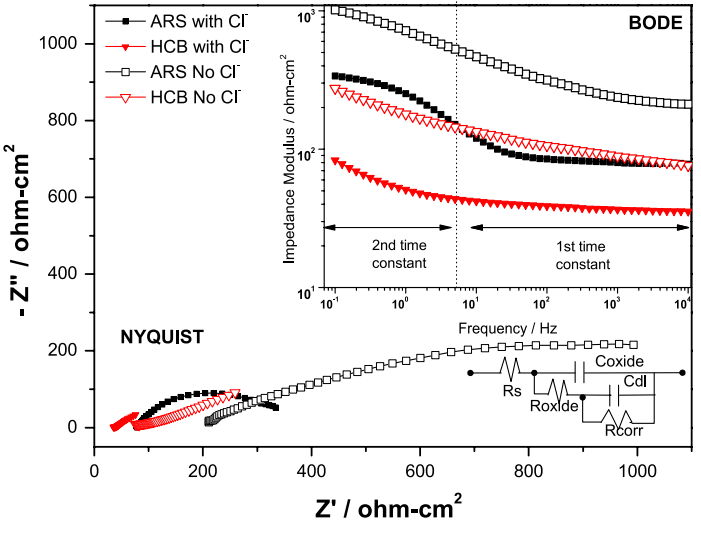

Figure 4. Impedance diagrams at 168 h of testing with and without dechlorination process of artificially rusted samples and historical cannon ball covered with Renaissance Wax.

Table 3. Electrochemical parameters of the ARS and HCB samples with and without Cl- removal treatment (results related to Figure 4).

Samples	$R_{\text{rust+wax /168 h}}$ (Ω cm^2)	Rust+wax resistivity $\rho_{\text{rust+wax}}$ (mohm-cm)	Porosity (%) $\rho_{\text{NaCl}}/\rho_{\text{rust'+wax}}$ at 168 h
ARS with Cl$^-$	90.1 ± 3.2	2.3 ± 0. 65	2.17 ± 0.32
ARS No Cl$^-$	406.8 ± 2.7	10.3 ± 1.32	0.48 ± 0.15
HCB with Cl$^-$	45.1 ± 5.7	1.2 ± 0.2	4.05 ± 1.23
HCB No Cl$^-$	107.8 ± 3.1	2.9 ± 0.6	1.69 ± 0.65

the solution resistance and the C_{oxide} and R_{oxide} refers to the iron rust+wax capacitance and resistance. The C_{dl} and R_{corr} refer to the corrosion mechanism of the substrate.

For both cases which contained chloride (before the dechlorination process) the $R_{\text{rust-wax}}$, attributed to high frequencies, had an average value of between 50 and 100 Ω cm^2, whereas in dechlorinated cases the values of $R_{\text{rust-wax}}$ varied from 108 to 410 Ω cm^2, that is, the oxide resistance after chloride removal increased twice for ARS and four times for HCB. More information from the EIS data should be extracted in order to explain this result. Hence, the $R_{\text{rust-wax}}$ parameter was normalized by the value of the oxide thickness for each sample given that the rust+wax resistivity is expressed in mohm-cm. Table 3 shows this parameter as well as the calculation of the porosity percentage of the rust+wax (% = $\rho_{\text{NaCl}}/\rho_{\text{rust+wax}}$). As can be seen, the HCB before the dechlorination process exhibits the highest degree of porosity among all the samples and thus, the lowest rust+wax resistivity. This indicates that the HCB with chloride content and the commercial wax did not provide an effective barrier effect for longer exposure times due to high surface heterogeneities. On the other hand, the ARS subjected to the chloride removal process proved to have the lowest defective surface. Therefore, the low porosity of dechlorinated samples suggests modification of the rust morphology and thus, obtaining lower defect oxides. Since Renaissance Wax was applied to both samples, the rust morphology mainly determines the EIS performance. As reported in literature [32], the Renaissance Wax slows down the oxidation process of metals but does not necessarily contribute to the blockage of voids present inside the oxide morphology.

From the above results, it is clear that further investigation into the morphology features of the samples with and without chloride content (Figures 5, 6) is necessary. As shown in Figure 5(a) and (b), the HCB shows a completely different topography before and after treatment. The sample containing chloride (Figure 5(a)) depicts an agglomerate distribution throughout the entire sample with average size values of 10 μm. These agglomerates are spherical-shaped forms containing holes and superficial defects. However, the dechlorinated sample, Figure 5(b), is smoother with a homogeneous distribution of smaller particles that cover almost the entire surface although it is covered with cracks. These defects seem to be responsible for the low barrier properties indicated by Figure 4 and calculated with $R_{\text{rust-wax}}$. It is seen that cracks dominated the surface even with the application of the Rennaisance Wax. In addition, it is important to highlight that the microstructure of the rust layer in the HCB was completely destroyed after the dechlorination process since all oxide particles changed their superficial morphology as can be seen in Figure 5(b). The EDX spectrum for each sample (Figure 5(c) and (d)) is shown in order to confirm the composition of these surfaces. These spectra reveal an identical composition for both cases except for the chloride content, which notably decreased after the dechlorination process. This analysis confirms the effectiveness of the dechlorination process on the very low chloride anion content on the iron rust.

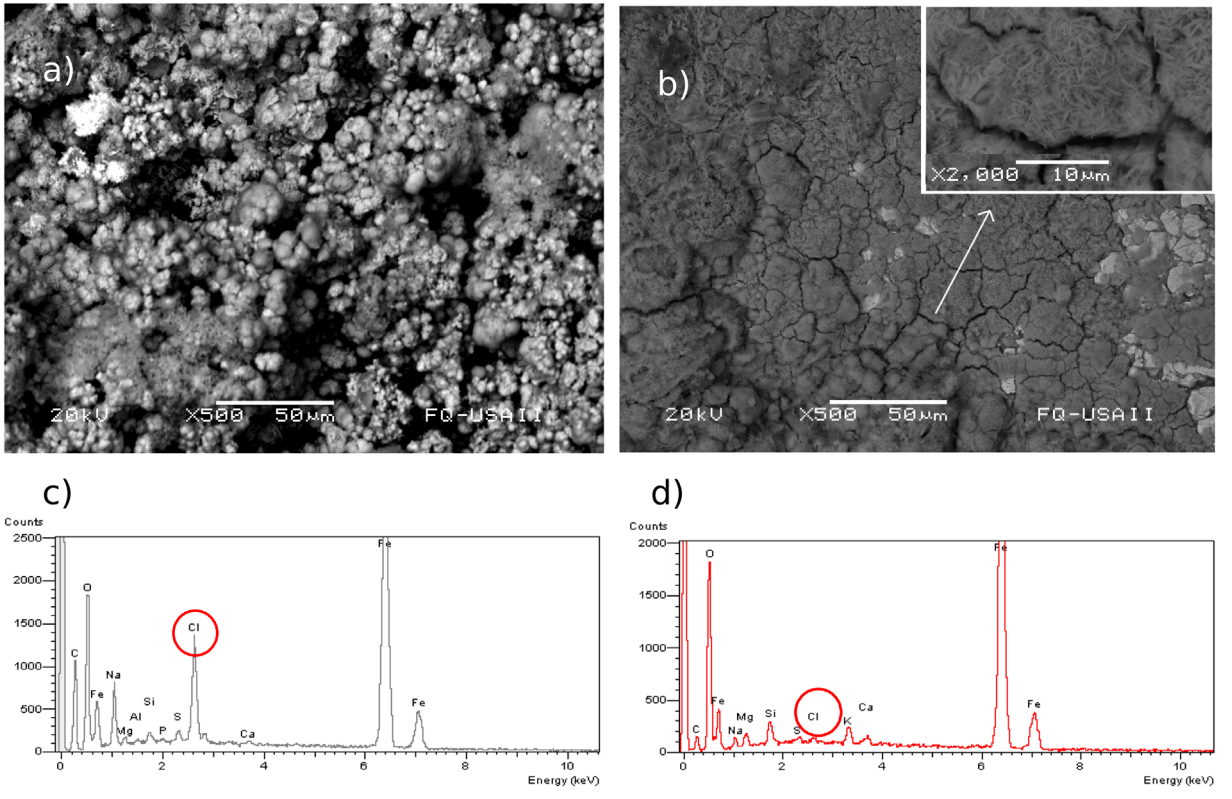

Figure 5. SEM/EDX results of cannon ball sample before (a), (c) and after (b), (d) the dechlorination process, respectively.

On the other hand, the ARS shows a random distribution of different morphology particles on the surface. Both lamellar-like particles and needle-like structures of variable size are seen (Figure 6(a)). Nevertheless, the dechlorinated sample also shows a homogenous distribution of the corrosion rust where a small flake-like structure can be found. The main feature of this sample is that superficial defects are much smaller than those observed for the HCB. A closer look at the surface of Figure 6(b) hardly reveals any scratches or cracks. This evidence shows that the chloride removal on rusted samples did not significantly modify the surface morphology because similar features of the oxide structure remained unaltered. Similar results of EDX to those obtained for the HCB were obtained in the ARS since the chloride anion content notably decreased after the dechlorination process, as can be seen in Figure 6(d) (after Cl^- removal).

The modification of the structural surface of the HCB was also sensitive to XRD analyses. Figure 7 shows the XRD patterns of all samples before and after the dechlorination process. As can be seen, the crystalline structure is modified after the chloride extraction procedure. The HCB before treatment shows different iron rust phases such as goethite, lepidocrocite, maghemite, akaganeite and hematite, however, after the chloride extraction procedure the main iron products were goethite and maghemite. Nevertheless, the main feature of the spectra after the dechlorination process is focused on a loss of crystallinity in the structure since the peaks of goethite are smaller and hardly identifiable at specific 2θ values. Furthermore, iron products such as lepidocrocite, akaganeite and hematite were not detectable along the spectra, that is, the dechlorination process removed these iron compounds.

Analogous results were obtained for the ARS. Before the dechlorination process, compounds such as potassium iron chloride, sodium iron oxide, sodium chloride and maghemite were identified, whereas after the chloride removal treatment, goethite and akaneite were identified as the major iron rust contributions as shown in Figure 7. However, these compounds did not lose their crystalline structure, nor did the HCB since all characteristic peaks of the identified compounds are clear and identifiable from $2\theta = 10°$ to $2\theta = 40°$ and from $2\theta = 60°$ to $2\theta = 70°$. That is, the crystalline modification was only focused on specific compounds. It would be ideal to confirm the effect of the dechlorination process on the structure of the iron oxides by calculating the average crystal size by means of a Scherrer equation, however, the spectra of the HCB did not allow for accurate measurement of the maximum peak height nor the width of the peaks of the remaining iron compounds. Therefore, the semi-quantitative phases of each compound before and after the chloride removal was evaluated following the procedure given by factor I/Ic of Evaluation 11.0 from software DiffracPlus 2005. Table 4 shows that the HCB did not have free chloride ions coming from NaCl but shows chloride content within the iron layer in the form of akaganeite and potassium iron chloride ($KFCl_4$). After the treatment, only maghemite and goethite remained as iron rust since the other iron compounds were removed and/or destroyed from the surface. As already explained, this modification completely changed the morphological features of the surface.

On the other hand, the ARS before treatment had NaCl debris, Cl^- containing compounds (silicate chloride and $KFCl_4$) and free Cl^- compounds (maghemite, γ-Fe_2O_3, and sodium iron oxide, Na_2FeO_4). After the chloride removal, only goethite and akaganeite mixed with NaCl crystals were detected. The fact that these two iron compounds were formed while the others disappeared suggests that the dechlorination process removed or

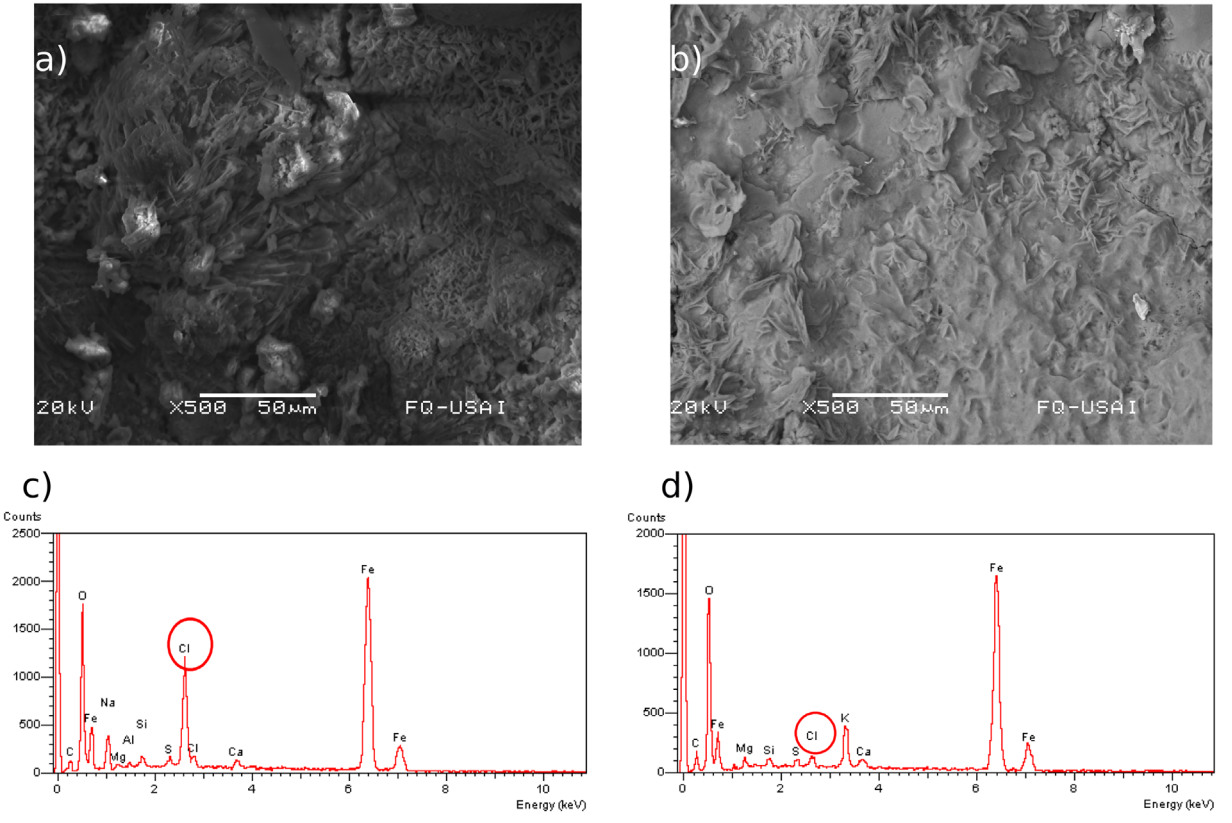

Figure 6. SEM/EDX results of artificially rusted sample before (a), (c) and after(b), (d) the dechlorination process.

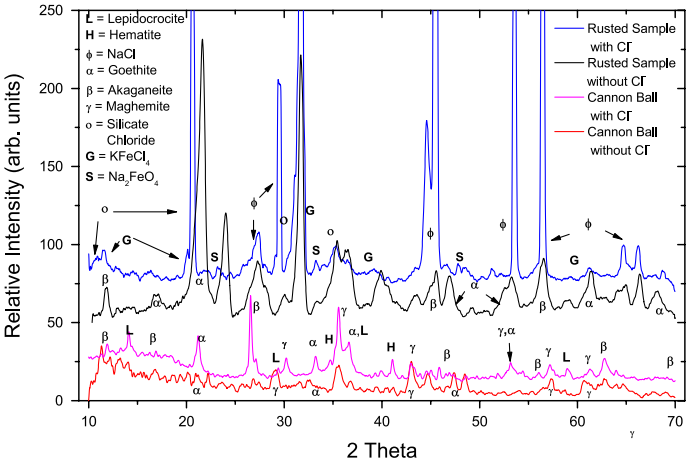

Figure 7. XRD pattern obtained for all samples, cannon ball and artificially rusted, with and without the dechlorination process.

Table 4. XRD semi-quantitative analysis of rusted samples and cannon ball artefacts.

	HCB with Cl^-	HCB without Cl^-	ARS with Cl^-	ARS without Cl^-
Sodium chloride	0	0	21.7	24.1
Maghemite	38.3	66.6	4.3	0
Goethite	30.3	33.4	0	56.9
Lepidocrocite	13.7	0	0	0
Akaganeite	9.6	0	0	19
Hematite	8.1	0	0	0
Silicate chloride	0	0	25.8	0
Sodium Iron Oxide	0	0	12	0
Potassium iron chloride	0	0	36.2	0
Total	100	100	100	100

destroyed the external rust layer and revealed a sub-superficial iron layer without modifying its crystalline structure.

Therefore, taking into account these XRD results along with the high Cl^- extraction amount (5 g/l) for the ARS, the chloride removal must be released to a bulk solution with relative ability, i.e. the chloride extracted from this oxide was absorbed at the surface of the iron layer, whereas the Cl^- extracted from the HCB was trapped within the crystalline structure, thus this Cl^- extraction is more associated with a deep profile rust layer than to a superficial structure as has been proposed and investigated by Kergourlay et al. [35], Reguer et al. [36] and Ståhl et al. [37]. For this reason, the difficulty of extracting Cl^- chlorides was reflected in the low chloride extraction efficiency (0.75 g/l).

In order to characterize this surface morphology in detail, the average roughness (Ra) for all samples was evaluated using mechanical profilometry (Figure 8). This value gives a picture of the arithmetic average of the profile deviations of roughness. As can be seen in Table 5, the Ra after the dechlorination process decreased in the ARS (obtained from Figure 8(b)) whereas the rugosity for the HCB increased (obtained from Figure 8(d)). A rougher surface is correlated with a more fractal system which means a system that shows low corrosion protection [38–40]. As already analysed, all defects generated and detected by

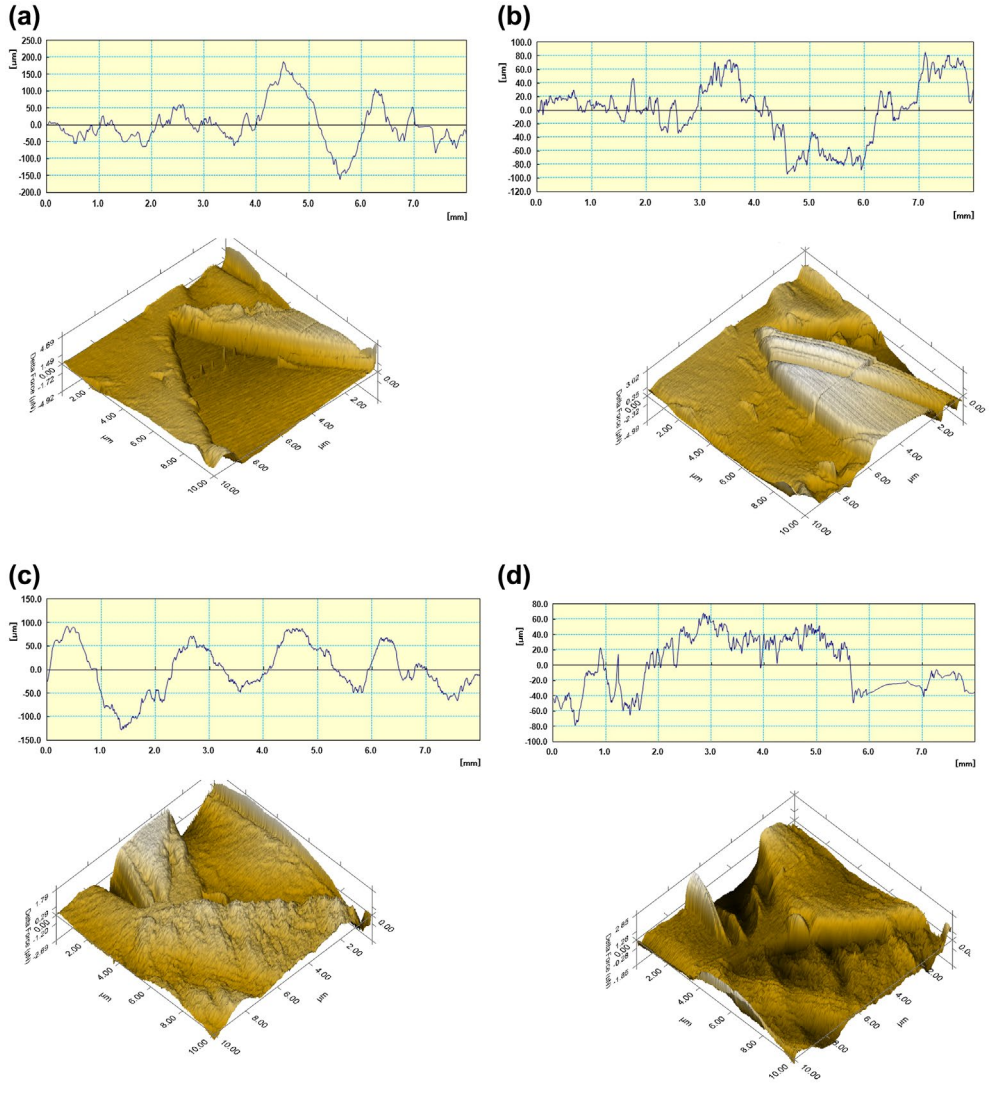

Figure 8. Marks of nanoindentation and mechanical profilometry of artificially rusted samples (a,b) and cannon balls (c,d).

Table 5. Mechanical and superficial parameters of the ARS and HCB samples.

	Ra (µm)		Nano hardness/Stiffness (GPa)/(µN/nm)	
Samples	With Cl^-	Without Cl^-	With Cl^-	Without Cl^-
Rusted Sample (ARS)	53.76 ± 19.7	37.51 ± 4.6	0.35/66.7	0.021/5.46
Cannon Ball (HCB)	42.35 ± 13.4	51.62 ± 2.5	0.028/37.4	0.0012/0.95

SEM micrographs after the chloride extraction increased the rugosity profile of the surface, thus the adhesion of Renaissance Wax to the HCB was lower than that observed in the ARS.

Finally, since the iron rust from the HCB cracked after the dechlorination process, it indicates a higher degree of stiffness in the microstructure. For this reason, in order to

corroborate the change in brittleness, nanohardness tests were measured on all samples. Table 5 also summarizes the obtained data. As can be seen, the results indicate a decrease in nanohardness and stiffness for all samples after the dechlorination process, in both the HCB and ARS. However the HCB samples exhibited the lowest values of both properties. The fact that mechanical properties diminished after the dechlorination process does not imply a softer material but rather the contrary. It was observed and registered that the nanoindenter did not completely penetrate the rust layers since these oxides (mainly in the HCB) broke during testing. These very low values (in hardness and stiffness) as well as the images from Figure 8 indicate that the porous iron oxides were so stiff that the mechanical contact between the rust and the indenter caused immediate fracturing. For this reason, results after the dechlorination treatment do not correspond to real values of nanohardness and stiffness of oxide layers. Images from Figure 8 indicate that the mark of the indenter on the ARS before the dechlorination process was clearly smooth (Figure 8(a)). However, after the chloride removal treatment the mark of the indenter corresponds to an unstable layer where the indenter did not completely penetrate due to the instability of the rust layer (Figure 8(b)). On the other hand, the HCB images (Figure 8c and d) show that the indenter could penetrate the sample before the chloride extraction but it was not possible to do so after the treatment since cracks and grooves appeared throughout the surface during the test (Figure 8(d)). The degree of stiffness was considerably high on the HCB artefact compared to the ARS. Therefore, the nanohardness results provide further evidence that the chloride extraction treatment on iron oxide layers causes a higher degree of stiffness on the rust layers.

Conclusions

Two types of ferrous rusted materials were subjected to a dechlorination process at –1.2 V (SCE), a historical cannon ball (HCB) and an artificially rusted low carbon steel (ARS). These objects displayed different morphology before chloride removal which was modified after dechlorination treatment. SEM and XRD spectra reveal that the chloride removal procedure caused a loss in crystallinity for the HCB with voids and cracks, whereas the ARS maintained their structural form. These results, along with the diffusion coefficient data (D_{Cl}), indicate that the chloride extraction, which followed Fick's second law of diffusion, was carried out from superficial layers for ARS and from the inner rust structure of the HCB respectively. After the dechlorination process the HCB exhibited the highest degree of stiffness as shown in nanohardness tests. Electrochemical tests and mechanical profilometry demonstrated that the ARS exhibited higher corrosion resistance after chloride removal. Since rust layers on the HCB were cracked, the degree of protection was poorer.

Therefore, the dechlorination treatment at –1.2 V (SCE) should take into account the initial morphology of historical artefacts in order to avoid harmful defects in the rust layer, so as to prevent damaging properties such as corrosion resistance and other mechanical properties.

Acknowledgements

Rebecca Jaimes Ramírez acknowledges Programa de Becas Posdoctorales from DGAPA, Universidad Nacional Autónoma de México 2016–2017, México and Miguel A. Hernández acknowledges the PAPIIT project at the DGAPA, Universidad Nacional Autónoma de México IN114316. The authors acknowledge Ivan Flores Acevedo and Dr. Bernardo F. Campillo for the nano-measurements facilities.

Disclosure statement

No potential conflict of interest was reported by the authors.

ORCID

R. Parra http://orcid.org/0000-0002-6337-2931
A. Covelo http://orcid.org/0000-0003-3053-9624

References

[1] Hernandez M, Hernandez-EscampaM, Abreu C, et al. Characterization of a Historical Cannonball from the Fortress of San Juan De Ulúa Exposed to a Marine Environment. Archaeometry. 2016;58:610–623.
[2] Oh SJ, Cook DC, Townsend HE. Atmospheric corrosion of different steels in marine, rural and industrial environments. Corros Sci. [Internet]. 1999 [cited 2014 Aug 6];41:1687–1702. Available from: http://www.sciencedirect.com/science/article/pii/S0010938X99000050.
[3] Guilminot E, Neff D, Rémazeilles C, et al. Influence of crucial parameters on the dechlorination treatments of ferrous objects from seawater. Stud Conserv. [Internet]. 2012;57:227–236. Available from: http://www.maneyonline.com/doi/abs/10.1179/2047058412Y.0000000011
[4] Hernandez-Escampa M, Gonzalez J, Uruchurtu-Chavarin J. Electrochemical assessment of the restoration and conservation of a heavily corroded archaeological iron artifact. J Appl Electrochem. 2010;40:345–356.
[5] Watkinson D, Rimmer MB, Kergourlay F. Alkaline desalination techniques for archaeological iron. Corros Conserv Cult Herit Met Artefacts [Internet]. 2013;407–433. Available from: http://www.sciencedirect.com/science/article/pii/B9781782421542500190
[6] Coelho JC, Oliveira CM, Carvalho MD, et al. The efficiency of electrochemical methods for the removal of chloride ions from iron marine archaeological objects: a comparative study. Mater Corros. 2014;65:38–44.
[7] Schmidt-Ott K, Boissonnas V. Low-pressure hydrogen plasma: an assessment of its application on archaeological iron. Stud Conserv. 2002;47:81–87.
[8] Watkinson D, Rimmer M, Kasztovszky Z, et al. The use of neutron analysis techniques for detecting the concentration and distribution of chloride ions in archaeological iron. Archaeometry. 2014;56:841–859.
[9] Turgoose S. Post-excavation changes in iron antiquities. Stud Conserv. [Internet]. 1982 [cited 2016 Sep 22];27:97. Available from: http://www.jstor.org/stable/1506144?origin=crossref
[10] Knight B. why do some iron objects break up in store? In: Clarke RW, Blacksaw SM, editors. Proceedings of a Symposium; 1980 Jul 4; Greenwich; 1982. p. 50–51.
[11] Castellote M, Andrade C, Alonso C. Electrochemical removal of chlorides: modelling of the extraction, resulting profiles and determination of the efficient time of treatment. Cem Concr Res. 2000;30:615–621.
[12] Andrade C, Castellote M, Sarría J, et al. Evolution of pore solution chemistry, electro-osmosis and rebar corrosion rate induced by realkalisation. Mater Struct. 1999;32:427–436.
[13] Rimmer M, Watkinson D, Wang Q. The efficiency of chloride extraction from archaeological iron objects using deoxygenated alkaline solutions. Stud Conserv. [Internet]. 2012;57:29–41. DOI:10.1179/2047058411Y.0000000005
[14] Watkinson D. Chloride extraction from archaeological iron: comparative treatment efficiencies. In: Roy A, Smith P, editors Archaeological conservation and its consequences Preparation of Contributions to the Copenhagen Congress; 1996 Aug 26–30; London: International Institute for Conservation; 1996. p. 208–212.
[15] Watkinson D. Degree of mineralization: its significance for the stability and treatment of excavated ironwork. Stud Conserv. 1983;28:85–90.

[16] Rinuy A, Schweizer F. Methodes de conservation d'objets de fouilles en fer. Etude quantitative comparee de l'elimination des chlorures. Stud Conserv. 1981;26:29–41.
[17] North NA, Pearson C. Thermal decomposition of FeOCl and marine cast iron corrosion products. Stud Conserv. 1977;22:146–157.
[18] Plenderleith HJ, Werner AEA. The conservation of antiquities and works of art: treatment, repair, and restoration. London: Oxford University Press; 1972.
[19] Bertholon R, Lacoudre C, Montlucon N, et al. L'Electrolyse appliquée à la conservation d'un canon en fer forgé du XVIe siècle. Cah d'Archéologie sub-Aquat. 1989;VIII:5–18.
[20] Rinuy A, Schweizer F. Application of the alkaline sulphite treatment to archaeological iron: a comparative study of different desalination methods of conservation of iron. In: Bradshaw S, Clarke R, editor. Conservation of Iron. National Maritime Museum Monograph Reports; London: National Maritime Museum; 1982. p. 44–49.
[21] North N, Pearson C. Alkaline sulphite reduction treatment of marine iron. ICOM Committee for Conservation 4th Triennial Meeting; Venice, Italy; 1975. p. 1–14.
[22] Gilberg MR, Seeley NJ. The alkaline sodium sulphite reduction process for archaeological iron: a closer look. Stud Conserv. 1982;27:180–184.
[23] Rimmer M, Watkinson D, Wang Q. The impact of chloride desalination on the corrosion rate of archaeological iron. Stud Conserv [Internet]. 2013;58:326–337. DOI:10.1179/2047058412Y.0000000068
[24] Bayle M, de Viviés P, Memet JB, et al. Corrosion product transformations in alkaline baths under pressure and high temperature: the sub-critical stabilisation of marine iron artefacts stored under atmospheric conditions. Mater Corros. 2016;67:190–199.
[25] Drews MJ, González-Pereyra N, Mardikian P, et al. The application of subcritical fluids for the stabilization of marine archaeological iron. Stud Conserv. 2013;58:314–325.
[26] González NG, Mardikian P, Näsänen L, et al. 20 – The use of subcritical fluids for the stabilisation of archaeological iron: an overview [Internet]. Eur Fed Corros Ser;2013. Available from: http://www.sciencedirect.com/science/article/pii/B9781782421542500207.
[27] ASTM D1141 – 98. 2013 Standard practice for the preparation of substitute ocean water. B. Stand. Vol. 11.02. ASTM International; 2003.
[28] Degrigny C, Spiteri L. Electrochemical monitoring of marine iron artefacts during their storage/stabilisation in alkaline solutions. In: Ashton J, Hallam D, editor. Proceedings of the ICOM-CC Metal WG interim meeting National Museum of Australia, Canberra, METAL04; Australia; 2004. p. 315–331.
[29] Liu J, Li Y, Wu M. Electrochemical methods for chloride removal from simulated cast iron artefacts. Stud Conserv. 2008;53:41–48.
[30] Leng A, Streckel H, Stratmann M. The delamination of polymeric coatings from steel. Part 2: first stage of delamination, effect of type and concentration of cations on delamination, chemical analysis of the interface. Corros Sci. 1998;41:579–597.
[31] Fuentes-Azcatl R, Barbosa MC. Sodium Chloride, NaCl/ε: new force field. J Phys Chem B [Internet]. 2016;acs.jpcb.5b12584. Available from: http://pubs.acs.org/doi/abs/10.1021/acs.jpcb.5b12584
[32] Swartz N, Clare TL. On the protective nature of wax coatings for culturally significant outdoor metalworks: microstructural flaws, oxidative chances, and barrier properties. J Am Inst Conserv. 2015;54:181–201.
[33] Considine B, Wolfe J, Posner K, et al. Conserving outdoor sculpture: the stark collection at the getty center. Los Angeles, CA: Getty Publications; 2010.
[34] Murray JN, Hack HP. Long-term testing of epoxy-coated steel in ASTM seawater using electrochemical impedance spectroscopy. Corrosion. 1991;47:480–489.
[35] Kergourlay F, Rémazeilles C, Neff D, et al. Mechanisms of the dechlorination of iron archaeological artefacts extracted from seawater. Corros Sci. [Internet]. 2011;53:2474–2483. DOI:10.1016/j.corsci.2011.04.003
[36] Reguer S, Mirambet F, Dooryhee E, et al. Structural evidence for the desalination of akaganeite in the preservation of iron archaeological objects, using synchrotron X-ray powder diffraction

and absorption spectroscopy. Corros Sci [Internet]. 2009;51:2795–2802. DOI:10.1016/j.corsci.2009.07.012

[37] Ståhl K, Nielsen K, Jiang J, et al. On the akaganeite crystal structure, phase transformations and possible role in post-excavational corrosion of iron artifacts. Corros Sci. 2003;45:2563–2575.

[38] Hernandez M, Inti-Ramos O, Guadalupe-Bañuelos J, et al. Correlation of high-hydrophobic sol-gel coatings with electrochemical and morphological measurements deposited on AA2024. Surf Interf Anal. 2016;48.

[39] Mahjani MG, Moshrefi R, Sharifi-Viand A, et al. Surface investigation by electrochemical methods and application of chaos theory and fractal geometry. Chaos Solitons Fractals [Internet]. 2016;91:598–603. DOI:10.1016/j.chaos.2016.08.011

[40] Hermoso-Diaz IA, Gonzalez-Rodriguez JG, Uruchurtu-Chavarin J. Use of EIS and electrochemical noise fractal analysis to study salvia hispanica as green corrosion inhibitor for carbon steel. Int J Electrochem Sci. 2016;11:4253–4266.

Appendix 1

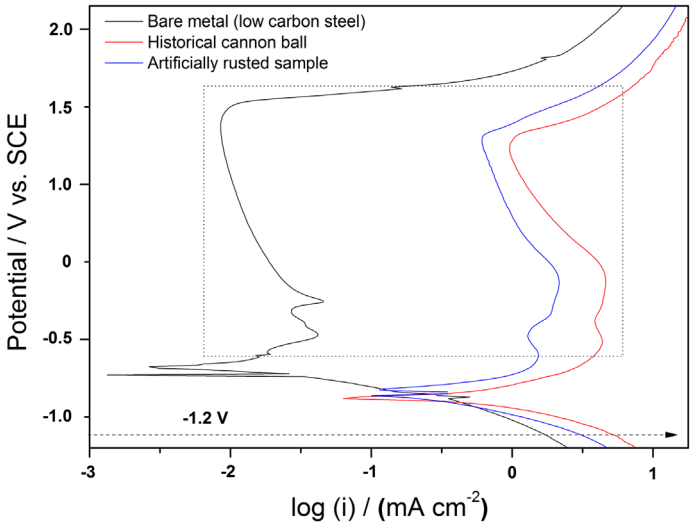

Figure A1. Polarization curves for bare metal, historical cannon ball and artificially rusted sample in sodium hydroxide solution.